Finite-size scaling of geometric renormalization flows in complex networks

Dan Chen [1], Housheng Su [1,*], Xiaofan Wang [2], Gui-Jun Pan [3], and Guanrong Chen [4]

[1]*School of Artificial Intelligence and Automation, Image Processing and Intelligent Control Key Laboratory of Education Ministry of China, Huazhong University of Science and Technology, Wuhan 430074, China*
[2]*Department of Automation, Shanghai University, Shanghai 200072, China*
[3]*Faculty of Physics and Electronic Science, Hubei University, Wuhan 430062, China*
[4]*Department of Electronic Engineering, City University of Hong Kong, 999077, Hong Kong*

Some characteristics of complex networks need to be derived from global knowledge of the network topologies, which challenges the practice for studying many large-scale real-world networks. Recently, the geometric renormalization technique has provided a good approximation framework to significantly reduce the size and complexity of a network while retaining its "slow" degrees of freedom. However, due to the finite-size effect of real networks, excessive renormalization iterations will eventually cause these important "slow" degrees of freedom to be filtered out. In this paper, we systematically investigate the finite-size scaling of structural and dynamical observables in geometric renormalization flows of both synthetic and real evolutionary networks. Our results show that these observables can be well characterized by a certain scaling function. Specifically, we show that the critical exponent implied by the scaling function is independent of these observables but depends only on the structural properties of the network. To a certain extent, the results of this paper are of great significance for predicting the observable quantities of large-scale real systems and further suggest that the potential scale invariance of many real-world networks is often masked by finite-size effects.

I. INTRODUCTION

Complex networks have attracted considerable attention from various disciplines such as mathematics, physics, biology, engineering, computer science, and others [1]. Its emergence was due to the discovery that associated with a real system there exists a corresponding network which can well define the interactions among the system components [2]. Because of this, one can better understand the structural and functional properties of the real system. In particular, by studying the topology of the network associated with a real system, some small-world properties [3] and scale-free properties [4] were identified. Consequently, their functional performances could be further studied, including synchronization [5,6], observability and controllability [7–9], reaction-diffusion [10], navigation [11], transportation [12,13], and many other dynamic behaviors.

However, exploring the network structural and functional properties also faces many challenges. For example, the evolutions of real-world networks usually lead to more complicated interactions and increasing numbers of nodes and edges, causing more difficulties for the investigations. In the past two decades, the renormalization technique [14,15] was found to be very effective for tackling the troublesome problem. This framework significantly reduces the size and the complexity of a large-scale network by retaining the "slow" degrees of freedom in the network, while integrating the rest together. In

so doing, smaller networks can be used to approximate the initially large ones. By performing a coarse-graining procedure for a spatially embedded scale-free network, it was shown [16] that a smaller network can maintain important structural characteristics of the original one. Based on random walks, a coarse-graining method was proposed [17] to reduce the size of a network, but retain most spectral properties of the original network through an iteration process. Furthermore, using the shortest path-length measure of a network, a box-covering technique was presented [18–20] for reducing the size of the network. It was shown that the iteration process can keep an approximately identical degree distribution of the network, which was verified by some real-world networks. Such a property is known as the network self-similarity [18]. In the following years, the box-covering technique had significant influence on the research of fractality and self-similarity [21–23], as well as flows and fixed points [24–26], of various complex networks.

It was observed that, for networks with small-world or even ultra-small-world properties, the transformation method based on shortest path-length cannot be effectively applied to study their structural symmetry and functional invariance. Therefore, a geometric renormalization (RGN) framework was proposed [27], embedded in a hidden metric space [28–33], which provides deep insights for studying the structural symmetry of complex networks. This framework is proved capable of preserving both structural and dynamical characteristics of scale-free networks, such as degree distribution, clustering spectrum, dynamics, and navigability, to a certain extent of accuracy within an appropriate number

*shs@hust.edu.cn

of iterations. Due to the finite-size effect on such networks, however, excessive RGN iterations will eventually result in a large deviation of the network features from the original ones.

To further explore the variation of the characteristics of a network in the RGN iteration process, this paper reports a comprehensive study of the finite-size scaling (FSS) behavior of the structural and dynamical observables in renormalization flows of synthetic and real evolutionary networks. For complex systems (networks), because the infinite size limit cannot be reached in the actual numerical simulation process, it is often observed that the behavior of the system deviates from the thermodynamic limit behavior. FSS, developed in the field of critical phenomena and renormalization groups, is an effective tool for analyzing and predicting the structural and dynamic behavior of finite systems. Specifically, we consider networks in small-world phase, non-small-world phase, and their critical regions, respectively, and perform FSS analyses of their structural and dynamic observables. Our results show that these observables can be characterized by a certain scaling function, and the exponent implied by the scaling function is independent of these observables but depends only on the structural properties of the network. We have verified the effectiveness of this conclusion via some real evolutionary networks, which provides further evidence for the predictive power of synthetic models to real systems.

The rest of this paper is structured as follows. In Sec. II we first review the average degree behavior of the $\mathbb{S}^1$ network model in different parameter regions through the RGN transformation process. Then we introduce the structure observables and dynamics observables of the network in detail. In Sec. III we perform FSS analysis on eight observables of $\mathbb{S}^1$ type of synthetic networks and real evolutionary networks, respectively. Finally, the discussion and the conclusion are given in Sec. IV and Sec. V, respectively.

II. PRELIMINARIES

A. $\mathbb{S}^1$ geometric models

A network can be embedded into a hidden metric space [28–30] based on the distance between nodes in the space, where the edges between nodes are dominated by popularity and similarity dimensions [31]. To be precise, popularity is directly related to the degrees of the nodes, while similarity is the sum of many other attributes that can regulate the possibility of interaction between nodes [27]. The model generated by these two mechanisms can clearly explain some universal properties of real networks, such as the structural complexity, evolutionary mechanism, and dynamical behaviors.

Consider a simple one-dimensional $\mathbb{S}^1$ geometric model [28], in which N nodes are placed on the circle of radius R. Each node i is dominated by two latent variables: one is the angle θ_i of the node i in the circle coordinates, used as the similarity measure, and the other is the hidden degree value κ_i, which is associated with the prevalence of the node and is proportional to the desired degree of the node in the network. In the model, θ_i is uniformly randomly taken from the interval $[0, 2\pi)$, and the value of κ_i satisfies the probability density function $\phi(\kappa) = (\nu - 1)\kappa_0^{\nu-1}\kappa^{-\nu}$, $\kappa \geqslant \kappa_0 = \langle k \rangle(\nu - 2)/(\nu - 1)$, and $\nu > 2$. Therefore, for nodes with large degrees, the
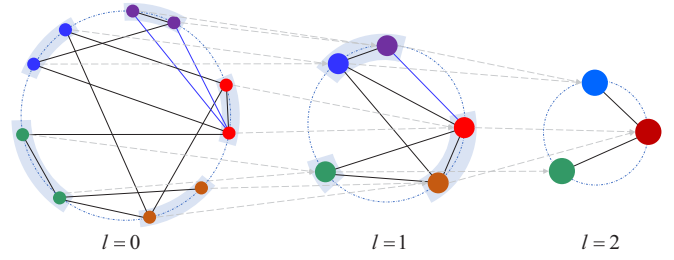

FIG. 1. The RGN transformation process of a weighted $\mathbb{S}^1$ geometric model. Starting from the initial network ($l = 0$), the nonoverlapping coarse-graining block (the shadowed areas in the figure) consisting of s continuous nodes is defined along the circle, and the dashed lines with arrows map the nodes in the block to their supernodes in layer $l + 1$. The straight solid lines in each layer represent the links between nodes, and two supernodes in layer $l + 1$ will be connected only if and only if a node in one coarse-graining block in layer l is connected to a node in another coarse-graining block. The figure shows the case of $s = 2$, s can be set to a larger value during the actual transformation process. Furthermore, for each layer of the network, when the total number of nodes is not divisible by s, the number of nodes contained in the last coarse-graining block in the layer will be less than s, and it will still be mapped to the supernode in the next layer.

observed degree distribution is approximately the same as $\phi(\kappa)$, i.e., $\Phi(k) \sim k^{-\nu}$. The radius R of the circle is proportional to the total number of nodes, N. For simplicity, set $N = 2\pi R$, which ensures that the average density of the nodes on the circle is equal to 1. The probability of connecting two nodes in hidden coordinates (θ_i, κ_i) and (θ_j, κ_j) on the circle is given by

$$p_{ij} = \frac{1}{1 + \psi_{ij}^\sigma} = \frac{1}{1 + \left[\frac{d(\theta_i,\theta_j)}{\mu\kappa_i\kappa_j}\right]^\sigma}, \quad (1)$$

where $d(\theta_i, \theta_j) = R\Delta\theta_{ij}$ is the geodesic distance between nodes i and j on the circle, and $\Delta\theta_{ij} = \pi - |\pi - |\theta_i - \theta_j||$. Equation (1) indicates that the connection probability between nodes increases with the product of the hidden degrees, but decreases with the increase of their distance along the circle [27]. The parameter μ controls the observed average degree of the network, and the parameter σ controls the average clustering coefficient of the network, such that the larger the value is and the smaller the effective distance is, the more advantageous it is to the increase of the average clustering in the network [28].

B. Average degree behaviors in geometric renormalization flows of the $\mathbb{S}^1$ model

In [27] a RGN framework (see Fig. 1) for complex networks is defined based on a hidden metric space [28–31]. Specifically, the $\mathbb{S}^1$ model is generated according to Eq. (1), and the distribution of nodes on the circle depends on their angular coordinates. The closer the angular coordinates are, the more similar the two nodes are considered to be. Once the $\mathbb{S}^1$ model is generated, the next step is to define nonoverlapping coarse-graining blocks along the circle and each block containing s contiguous nodes. The idea of RGN is to abstract (coarse-graining) these s nodes with

similar angular coordinates into one node (supernode) to get a smaller replica network. In addition, whether there are edges between supernodes depends on whether there are edges between block nodes before coarse graining. This principle is the same as that followed by the box-covering renormalization technique presented by Song *et al* [18]. The node's latent variables $(\kappa_{i,l+1}, \theta_{i,l+1})$ of the layer $l+1$ depend on the node's $(\kappa_{j,l}, \theta_{j,l})$ of the layer l, which satisfy $\kappa_{i,l+1} = [\sum_{j=1}^{s}(\kappa_{j,l})^{\sigma}]^{1/\sigma}$, $\theta_{i,l+1} = [\sum_{j=1}^{s}(\theta_{j,l}\kappa_{j,l})^{\sigma} / \sum_{j=1}^{s}(\kappa_{j,l})^{\sigma}]^{1/\sigma}$, García-Pérez *et al.* [27] have theoretically proved this result.

This RGN transformation has a good characteristic that it can well predict the average degree behavior of a large-scale network in the RGN flow process. Taking the $\mathbb{S}^1$ model for example, in [27], the average degree is shown to approximate satisfactorily an exponential relation along the RGN flow, as

$$\langle k \rangle_l = s^{\alpha} \langle k \rangle_{l-1}, \tag{2}$$

where the exponent α depends on the parameters ν and σ, with

$$\alpha = \begin{cases} \frac{2}{\nu-1} - 1, & 0 < \nu - 1 \leqslant \sigma, \\ \frac{2}{\sigma} - 1, & \sigma \leqslant \nu - 1 < 2\sigma. \end{cases} \tag{3}$$

According to Eq. (3), the $\mathbb{S}^1$ model can be roughly divided into three regions [27]:

I: $\nu < 3$ or $\sigma < 2$ and $\alpha > 0$, which corresponds to the small-world phase. Along the direction of the RGN flow, the network eventually approaches a highly connected graph. That is, in this region, the average degree of the network increases gradually along the RGN flow.

I to II: $\nu = 3$ and $\sigma \geqslant 2$ or $\sigma = 2$ and $\nu \geqslant 3$, namely, the network is at the critical region from the small-world phase to the non-small-world phase. According to Eq. (3), when the value of (ν, σ) is on the boundary line, $\alpha = 0$, the average degree of the network remains almost unchanged along the RGN flow.

II: $\nu > 3$ and $\sigma > 2$, namely, the network is located in the non-small-world phase, the exponent $\alpha < 0$, along the direction of the RGN flow, the renormalized network becomes more and more sparse and finally tends to a one-dimensional ring structure; as the renormalization process proceeds, the network eventually loses the small-world property.

III: $2\sigma < \nu - 1$, where the network becomes increasingly homogeneous as $s \to \infty$ (or $l \to \infty$), and consequently the network degree distribution lose its scale-freeness along the RGN flow. From simulations, it was found that the average degree of the renormalized layer has a similar behavior with Eq. (2), i.e., $\langle k \rangle_l = s^{\alpha} \langle k \rangle_{l-1}$.

Figure 2 shows the dependence of the average degree $\langle k \rangle_l$ of a particular network on the renormalized layer l within each region. Within regions I and III, $\langle k \rangle_l$ approximates an exponential growth. At the edge of the transition between regions I and II, the average degree $\langle k \rangle_l$ presents a tendency of slow increase with the increase of l, which gradually becomes saturated. Within region II, the average degree $\langle k \rangle_l$ approximates an exponential decay. The structure of the renormalized network is similar to a ring as a fixed point. The dashed lines show the result predicted by Eq. (3). Considering the randomness of the $\mathbb{S}^1$ model, there are some differences between
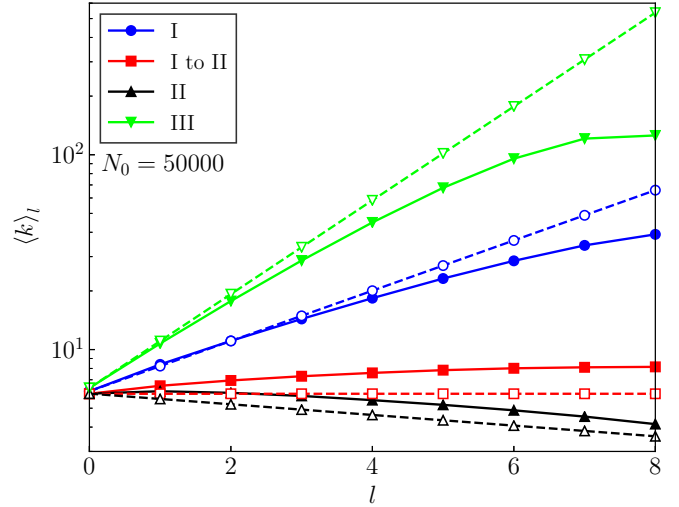

FIG. 2. The average degree $\langle k \rangle_l$ as a function of l for renormalized networks. Each solid curve represents the variation of the average degree of a particular network in the corresponding region along the RGN flow, and the dashed lines show the result predicted by Eq. (3). In region I, $(\nu, \sigma) = (2.5, 1.5)$. At the edge of the transition between regions I and II, $(\nu, \sigma) = (3.0, 2.5)$. In region II, $(\nu, \sigma) = (3.5, 2.5)$. In region III, $(\nu, \sigma) = (4.0, 1.1)$. The average hidden degree $\langle \kappa \rangle_0 \approx 6$ and the expected average degree $\langle k \rangle_0 \approx 6$ for all initial networks. The sizes of the initial networks are $N_0 = 50\,000$. All results are averaged over 10 independent realizations.

theoretical and simulation results. More importantly, due to the finite-size effect of the network, excessive renormalization will cause the average degree of the network to deviate seriously from the theoretical results. It can be seen from the Fig. 2 that the difference between the simulation results and the theoretical results gradually increases with the increase of l. We speculate that when the initial network size is large enough, the above phenomena show better consistency with $\langle k \rangle_l = s^{\alpha} \langle k \rangle_{l-1}$. Moreover, Fig. 2 further shows that the value of the parameter α can be used as a measure to distinguish between small-world and non-small-world network. That is, when $\alpha > 0$, the network in phase I or III belongs to a small-world network; when $\alpha \leqslant 0$, the network in phase II or in their critical region belongs to the non-small-world network.

C. Finite-size scaling behavior of observables in RGN flows

We carry out a comprehensive study of the FSS behavior of the structural and dynamical observables in renormalization flows of the typical $\mathbb{S}^1$ geometric network model [28]. First, an $\mathbb{S}^1$ network is generated with N_0 nodes and E_0 edges, denoted as G_0. Then, starting from G_0, nonoverlapping blocks of continuous nodes of size s are defined in the $\mathbb{S}^1$ circle [27]. Here $s = 2$ is chosen, and one-step RGN iteration is performed to obtain G_1. Consecutively, a layer-l renormalized network G_l is obtained after l steps of RGN iterations. The number of nodes in layer l is denoted by N_l, and the relative network size of layer l is $n_l = N_l/N_0$.

In the following, a RGN flow is tracked by eight observables. One is the normalized maximum degree of the
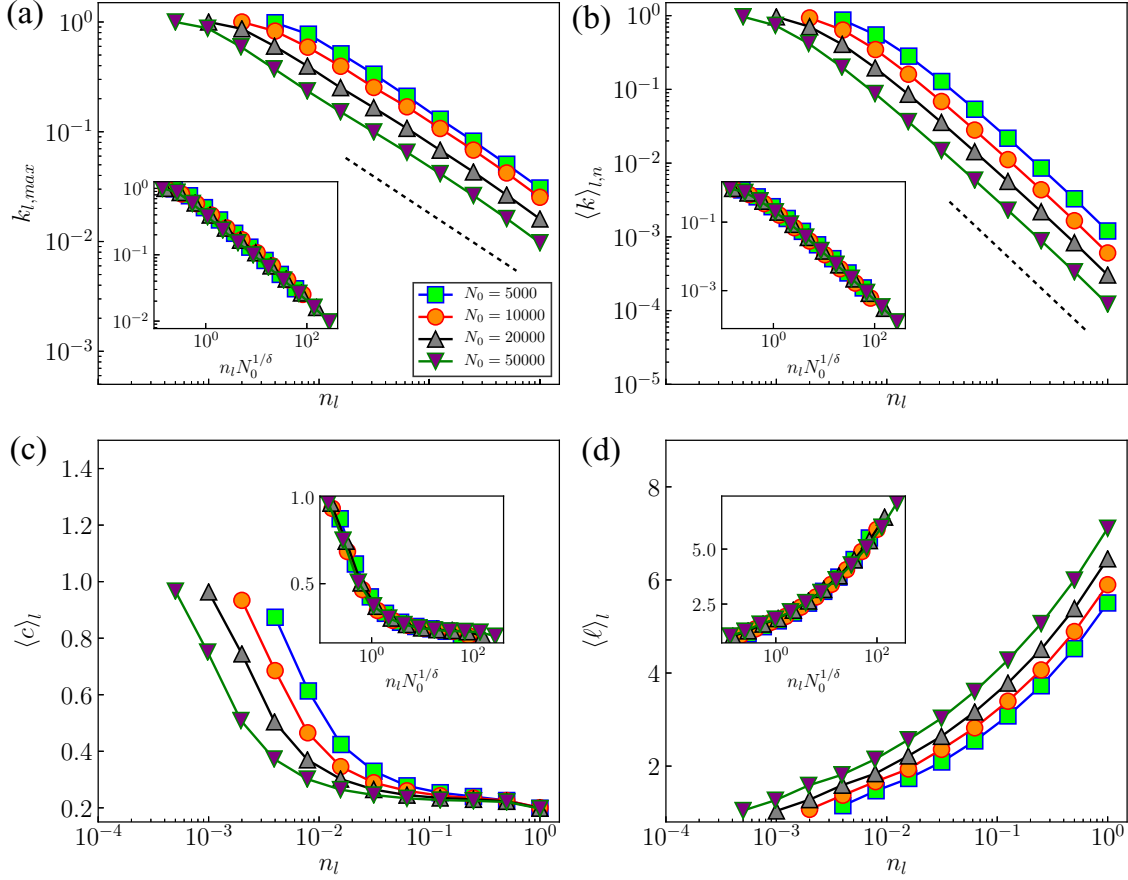
FIG. 3. FSS analysis of $\mathbb{S}^1$-network topological observables along the RGN flow. The main figures show each observable as a function of the variable n_l in the process of RGN transformation, and the inset shows their scaling functions related to the variable $n_l N_0^{1/\delta}$. Key parameters of the $\mathbb{S}^1$ network are $\nu = 2.5$ and $\sigma = 1.5$, respectively. These networks belong to phase I, and the scaling exponent corresponding to four observables is $\delta = 1.6(1)$. For observables $k_{l,\max}$ and $\langle k \rangle_{l,n}$, the black dashed lines show the predicted behavior of the scaling function. The average hidden degree $\langle \kappa \rangle_0 \approx 6$ and the expected average degree $\langle k \rangle_0 \approx 6$ for all initial networks. All results are averaged over 10 independent realizations.

renormalized network,

$$k_{l,\max} = \frac{K_l}{N_l - 1}, \tag{4}$$

where K_l is the maximum degree of the renormalized network G_l, and $N_l - 1$ is the maximum value that K_l may take. Another observable is the normalized average degree,

$$\langle k \rangle_{l,n} = \frac{\langle k \rangle_l}{N_l - 1}, \tag{5}$$

where $N_l - 1$ is the maximum value that $\langle k \rangle_l$ may take. The average clustering coefficient $\langle c \rangle_l$ and the average shortest path length $\langle \ell \rangle_l$ for the renormalized network G_l will also be considered below.

Regarding the above characteristics of networks, the FSS behavior is investigated through a box-covering procedure [24,25]. These observables are commonly used to characterize the basic topological properties of the network, referred to as topological observables of the network, as illustrated in Fig. 3.

Now, consider several other observables that represent global properties of networks. One is the normalized maxi-

mum eigenvalue of the Laplace matrix,

$$\lambda_{l,n}(L) = \frac{\Lambda_{l,n}(L)}{N_l}, \tag{6}$$

where $\Lambda_{l,n}(L)$ is the maximum eigenvalue of the Laplace matrix L of the renormalized network G_l, and N_l is the maximum value that $\Lambda_{l,n}(L)$ may take. For a connected network with at least one edge, it always satisfies $\Lambda_{l,n}(L) \geqslant K_l + 1$, where the equality holds if and only if $K_l = N_l - 1$ [34]. The first normalized nonzero eigenvalue of the Laplace matrix is

$$\lambda_{l,2}(L) = \frac{\Lambda_{l,2}(L)}{N_l}, \tag{7}$$

where $\Lambda_{l,2}(L)$ is the first nonzero eigenvalue of the Laplace matrix L of the renormalized network G_l, and N_l is the maximum value that $\Lambda_{l,2}(L)$ may take. To some extent, the functional properties of a network can be optimized by increasing the value of $\Lambda_{l,2}(L)$. For instance, maximizing $\Lambda_{l,2}(L)$ can maximize the rate of convergence to the network homogeneous state for undirected networks [35].

Also, the $\mathbb{S}^1$ model parameters can be divided into three regions according to the diffusion time $1/\Lambda_{l,2}(L)$ as discussed earlier [27]. In the following, consider the ratio of the
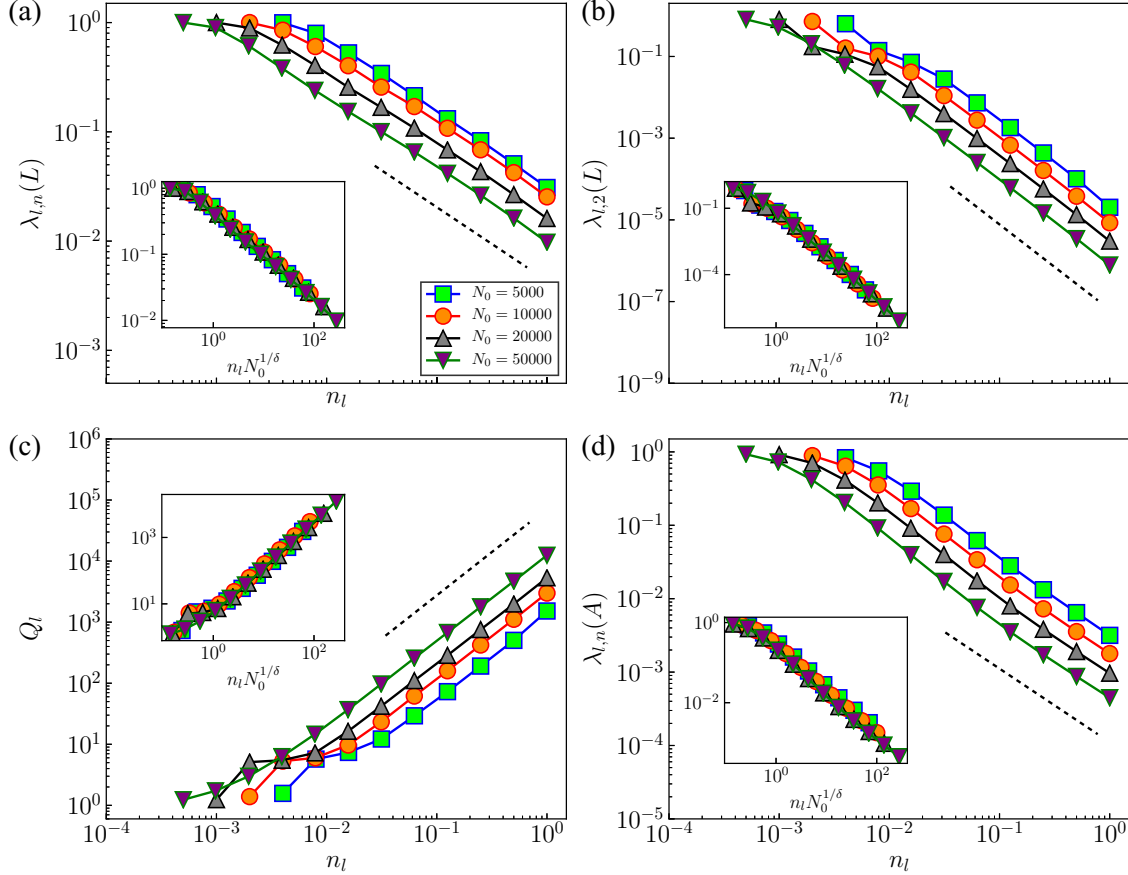
FIG. 4. FSS analysis of $\mathbb{S}^1$-network dynamic observables along the RGN flow. The main figures show each observable as a function of the variable n_l in the process of RGN transformation, and the inset shows their scaling functions related to the variable $n_l N_0^{1/\delta}$. Key parameters of the $\mathbb{S}^1$ network are $\nu = 2.5$ and $\sigma = 1.5$, respectively. These networks belong to phase I, and the scaling exponent corresponding to four observables is $\delta = 1.6(1)$. For all observables, the black dashed lines show the predicted behavior of the scaling function. The average hidden degree $\langle \kappa \rangle_0 \approx 6$ and the expected average degree $\langle k \rangle_0 \approx 6$ for all initial networks. All results are averaged over 10 independent realizations.

maximum eigenvalue of the Laplace matrix to the first nonzero eigenvalue [36–41],

$$Q_l = \frac{\lambda_{l,n}(L)}{\lambda_{l,2}(L)}, \tag{8}$$

which is related to the synchronizability [41,42] and stability [27] of the network synchronization process.

Lastly, the spectral properties of the network adjacency matrix determine the behavior of many dynamic processes, among which the largest eigenvalue of the adjacency matrix is an important one, and its normalized result is given by

$$\lambda_{l,n}(A) = \frac{\Lambda_{l,n}(A)}{N_l - 1}, \tag{9}$$

where $\Lambda_{l,n}(A)$ is the largest eigenvalue of the adjacency matrix A of G_l, and $N_l - 1$ is the maximum value that $\Lambda_{l,n}(A)$ may take. Recently, the relationship between the maximum eigenvalue $\Lambda_{l,n}(A)$ and two network subgraphs was revealed for a large number of synthetic and real networks [43]. It also shows [44] the impact of $\Lambda_{l,n}(A)$ on two highly correlated dynamical models: one is epidemic spreading with threshold $\lambda_c = 1/\Lambda_{l,n}(A)$ and the other is synchronization of Kuramoto oscillators with threshold $\zeta_c = \zeta_0/\Lambda_{l,n}(A)$. In this context, the variables in Eqs. (6)–(9) have a critical effect on the dynamical

behavior of the network. For this reason, they are called dynamic observables of networks. Their FSS is shown in Fig. 4.

Next, along the directions of the RGN flows, FSS analysis is performed on eight network observables in regions I (small-world phase) and II (non-small-world phase), respectively. Specifically, the dependence of these observables on n_l is investigated for each layer of the renormalized network. The results indicate that these observables can be represented by a scaling function with $n_l N_0^{1/\delta}$ as the variable. More precisely, any observable $\mathcal{X}$ approximately satisfies

$$\mathcal{X} = f\left(n_l N_0^{1/\delta}\right), \tag{10}$$

where $f(\cdot)$ is a function depending on the initial network size and specific transformation used.

III. RESULTS

A. FSS of RGN flows in synthetic networks

Figure 3 shows the dependence of $k_{l,\max}$, $\langle k \rangle_{l,n}$, $\langle c \rangle_l$ and $\langle \ell \rangle_l$ on n_l for the $\mathbb{S}^1$ synthetic network. The inset shows each observable as a function of $n_l N_0^{1/\delta}$. The results show that the observable curves of networks with different sizes largely overlap. Specifically, in the small-world phase with

$(\nu, \sigma) = (2.5, 1.5)$, the scaling exponent $\delta \gg 1$ ($\delta \approx 1.6$; see Fig. 3), while in the non-small-world phase with $(\nu, \sigma) = (3.5, 2.5)$, the scaling exponent $\delta \approx 1$ (see Fig. S4 in the Supplemental Material [45]). The estimation method of exponent δ is shown in Fig. S1 and Refs. [46–48]. Interestingly, for $k_{l,\max}$ and $\langle k \rangle_{l,n}$, the results shown in Fig. 3 demonstrate that they are both approximately obey a power-law relationship with n_l, where the black dashed lines show the predicted behavior of the scaling function.

In the following, the power-law behaviors of these two observables are further discussed. Simulation results show that the maximum degree K_l of the renormalized network G_l and the maximum degree K_{l-1} of G_{l-1} are related as

$$K_l = s^\varepsilon K_{l-1} = \cdots = s^{l\varepsilon} K_0. \tag{11}$$

Since $n_l = N_l/N_0 = s^{-l}$, it follows that

$$
\begin{aligned}
k_{l,\max} &= \frac{K_l}{N_l - 1} \approx \frac{s^{l\varepsilon} K_0}{N_l} = \frac{n_l^{-\varepsilon} K_0}{n_l N_0} \\
&= \frac{n_l^{-(\varepsilon+1)} K_0}{N_0} \\
&\approx k_{0,\max} n_l^{-(\varepsilon+1)}. \tag{12}
\end{aligned}
$$

The above equation indicates that $k_{l,\max}$ approximately follows a power-law relation, $k_{l,\max} \sim n_l^{-\beta}$, where $\beta = \varepsilon + 1$. For the observed average degree $\langle k \rangle_l$ of the renormalized network G_l, when $\nu - 1 < 2\sigma$, it was shown [27] that the average degree approximately satisfies an exponential relation along the RGN flow, $\langle k \rangle_l = s^\alpha \langle k \rangle_{l-1}$, which yields

$$\langle k \rangle_l = s^\alpha \langle k \rangle_{l-1} = \cdots = s^{l\alpha} \langle k \rangle_0, \tag{13}$$

consequently,

$$
\begin{aligned}
\langle k \rangle_{l,n} &= \frac{\langle k \rangle_l}{N_l - 1} \approx \frac{s^{l\alpha} \langle k \rangle_0}{N_l} = \frac{n_l^{-\alpha} \langle k \rangle_0}{n_l N_0} \\
&= \frac{n_l^{-(\alpha+1)} \langle k \rangle_0}{N_0} \\
&\approx \langle k \rangle_{0,n} n_l^{-(\alpha+1)}. \tag{14}
\end{aligned}
$$

The above equation shows that, when $\nu - 1 < 2\sigma$, $\langle k \rangle_l$ approximately obeys a power-law relation, $\langle k \rangle_{l,n} \sim n_l^{-\eta}$, with $\eta = \alpha + 1$. For $\nu - 1 > 2\sigma$, through simulations it is found that the average degree $\langle k \rangle_l$ still approximately satisfies $\langle k \rangle_l = s^\alpha \langle k \rangle_{l-1}$, leading to $\langle k \rangle_{l,n} \sim n_l^{-\eta}$, with $\eta = \alpha + 1$. The values of β and η are given in Table S1 of the Supplemental Material [45].

Finally, consider the dependence of several dynamic observables on n_l [see Eqs. (6)–(9)], which depend on the spectral properties of the Laplace matrix and the adjacency matrix of the network, as shown in Fig. 4. To a certain extent, these observables are able to reflect some dynamical properties of a network, such as synchronization stability, diffusion time, and synchronization threshold of Kuramoto oscillator parameters. The inset of Fig. 4 shows the dependence of the observables on $n_l N_0^{1/\delta}$ for different sizes of networks, which is similar to the phenomenon presented in Fig. 3. More importantly, the exponent δ is also consistent with that in Fig. 3,
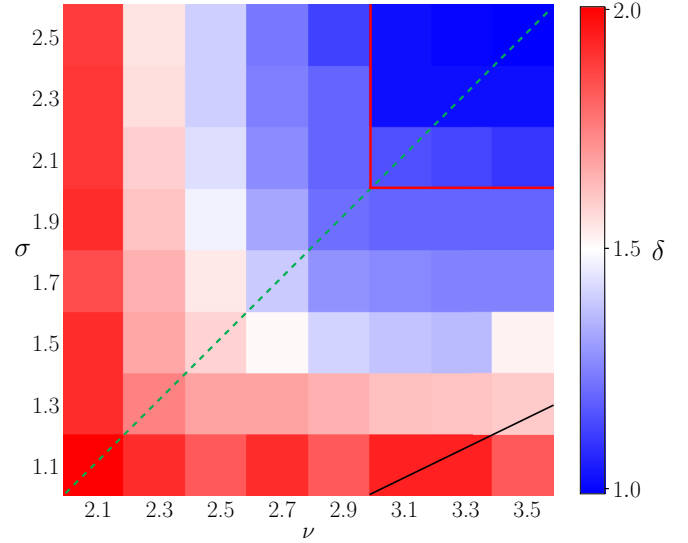

FIG. 5. The contour plot of the critical exponent δ. Only numerical results for the normalized average degree are given here, and our results show that other observables have very similar numerical results. The black and red solid lines in the figure are theoretical boundaries that separate these regions defined in Sec. II B. The results show that the phase diagram for δ here has a strong correlation with the phase diagram for α [see Eq. (3)] in the previous study [27].

namely, in the small-world phase, $\delta \gg 1$, and in the non-small-world phase, $\delta \approx 1$ (see Fig. S5 in the Supplemental Material [45]). The black dashed lines show the predicted behavior of the scaling function for each observable along the RGN flow. The corresponding power-law exponent values are listed in Table S1 of the Supplemental Material [45]. It is worth noting that these observables approximately obey power-law curves along the RGN flows, providing important guidance for predicting the structural and dynamical properties of large-scale networks. For instance, one can use the eigenvalue ratio Q_l of a renormalized smaller-size network to estimate the synchronizability of the initial large-scale network. To some extent, it can also be used to eliminate various consequences caused by the high complexity of large-scale networks. Furthermore, the results also show that for higher-dimensional embedded networks, by embedding a network into a D-dimensional ($D \geqslant 2$) space, the value of the exponent δ is consistent with that of the $\mathbb{S}^1$ model (see Figs. S8– S11 in the Supplemental Material [45]).

As a supplement, we provide a more robust result to support the above conclusions. Specifically, for each observable, we consider more parameters (ν, σ) combination and plot the associated contour map (heat map), as shown in Fig. 5. The horizontal and vertical coordinates correspond to parameters ν and σ, respectively, and the color level corresponds to the value of δ. Our results show that, for eight observables considered in this paper, they have very similar numerical results. In addition, similar to the conclusion in Ref. [27] [i.e., Eq. (3) in this paper], the phase diagram of the critical exponent δ can also be used as an auxiliary means to divide the phases of the network.

TABLE I. Topology characteristics of real evolutionary networks. For each network, we report the network name, the number of nodes of the largest connected component, the number of edges of the largest connected component, the value of the exponent ν, the value of the parameter σ, the average clustering coefficient, the phase of the network.

	Name	N	E	ν	σ	$\langle c \rangle$	Phase
1	IG5-9	538	4570	4.71	1.0056	0.0222	III
2	IG5-11	1692	22 110	3.10	1.0085	0.0003	III
3	IG5-13	4731	91 209	4.45	1.0096	0.0112	III
4	IG5-15	11 987	323 509	3.73	1.0062	0.0097	III
5	IG5-17	30 162	1 034 600	4.54	1.0066	0.0135	III
6	TF13	1302	11 044	6.05	1.0077	0.0356	III
7	TF14	3160	29 668	5.74	1.0070	0.0164	III
8	TF15	7742	79 848	5.43	1.0067	0.0081	III
9	TF16	19 321	215 942	5.14	1.0075	0.0035	III
10	TF17	48 630	585 951	4.96	1.0053	0.0018	III
11	Rajat06	10 922	18 061	2.30	2.3593	0.4438	I
12	Rajat07	14 842	24 571	2.27	2.3834	0.4439	I
13	Rajat08	19 362	32 081	2.25	2.3829	0.4440	I
14	Rajat09	24 482	40 591	2.24	2.4735	0.4440	I
15	Rajat10	30 202	50 101	2.22	2.4876	0.4441	I
16	Gnutella, 4 Aug. 2002	10 876	39 994	3.39	1.0061	0.0080	III
17	Gnutella, 25 Aug. 2002	22 663	54 693	4.36	1.0070	0.0090	III
18	Gnutella, 30 Aug. 2002	36 646	88 303	5.65	1.0065	0.0114	III
19	Gnutella, 31 Aug. 2002	62 561	147 878	4.74	1.0077	0.0101	III
20	Cage9	3534	19 030	6.16	1.5127	0.2095	III
21	Cage10	11 397	69 624	6.80	1.4405	0.1803	III
22	Cage11	39 082	260 320	6.46	1.4370	0.1736	III
23	Cage12	130 228	951 154	7.17	1.4232	0.1582	III
24	Maragal-2	549	4313	2.59	1.0058	0.1563	I
25	Maragal-3	1687	18 246	2.78	1.0071	0.1787	I
26	Maragal-5	4654	92 683	2.83	1.0055	0.1696	I
27	Maragal-6	21 255	536 283	2.90	1.0099	0.1208	I
28	AS-1998-01-02	3216	5705	2.35	1.0949	0.3311	I
29	AS-1999-12-06	6301	12 226	2.18	1.2041	0.4006	I
30	AS-2001-05-26	11 174	23 409	2.19	1.3095	0.4532	I
31	CAIDA-2004-01-05	16 301	32 955	2.21	1.0474	0.3585	I
32	CAIDA-2006-01-30	21 339	43 283	2.16	1.1383	0.3648	I
33	CAIDA-2007-11-12	26 389	52 861	2.16	1.1289	0.3325	I
34	Cond-Mat, 1995–1999	13 861	44 619	2.82	5.5954	0.7194	I
35	Cond-Mat, 1995–2003	27 519	116 181	2.61	3.8944	0.7107	I
36	Cond-Mat, 1995–2005	36 458	171 735	2.51	3.6290	0.7079	I
37	Socfb-UC64	6810	155 320	5.77	1.3660	0.2831	III
38	Socfb-UC61	13 736	442 169	5.37	1.3522	0.2714	III
39	Socfb-UC33	16 800	522 141	4.85	1.2898	0.2349	III

B. FSS of RGN flows in real evolutionary networks

As a common practice, it is necessary to verify the universality of the above conclusions with real networks, mostly small-world networks. Obviously, this brings up the problem that a single network has only one initial size N_0. To address this issue, some evolutionary network systems are employed, each of which eventually leads to a series of networks of different sizes over time, and these networks of the same type with different sizes are all approximately in the same phase on the (ν, σ) plane. Ten types of real evolutionary networks [49–53] (including 39 networks) are investigated, and the parameter σ value of each network is inferred according to an existing method [54]. The results show that these networks belong to small-world networks, that is, in phase I or III. In Table I we show the basic topology characteristics of 10 types

of real evolutionary networks [49–53], where the parameter ν is the approximate value obtained by fitting the tail of the degree distribution curve, and the parameter σ is a parameter necessary to embed the real network into the synthetic network, which is inferred by the method in [54]. The parameters ν and σ determine the position of each network in the (ν, σ) plane. Our results indicate that these networks are all in phase I or III, that is, they belong to small-world networks.

These networks are embedded into different $\mathbb{S}^1$ networks, and then the geometric renormalization transformation is performed. It is found that the eight observables curves of the same type but different sizes of the evolutionary networks overlap roughly, and the exponent δ is consistent with that of the synthetic network (small-world phase), i.e., $\delta \approx 2$. Take the IG5 evolutionary network [49] as an example. It has five
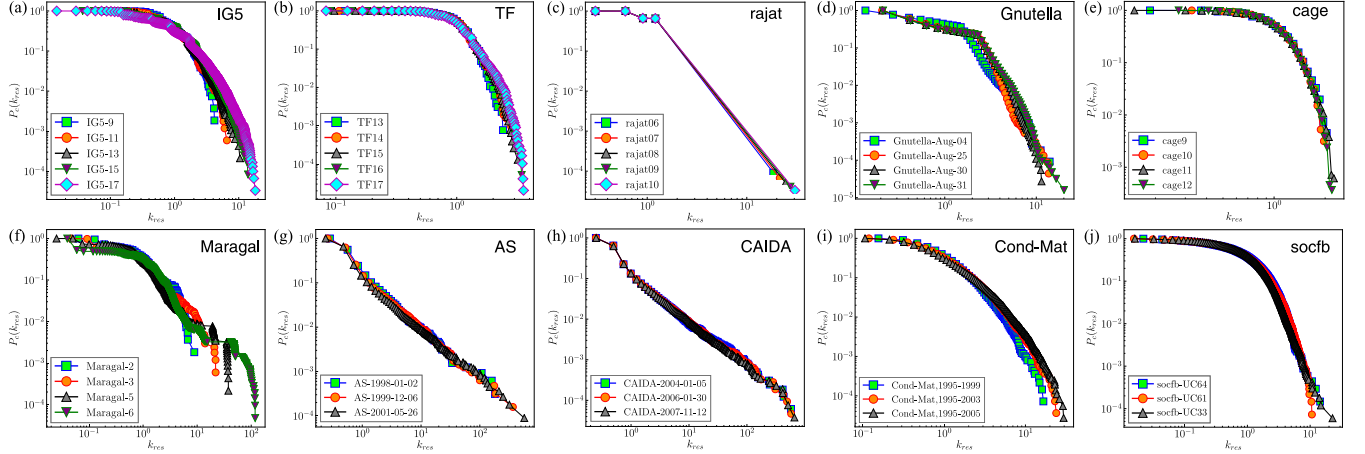
FIG. 6. Self-similarity of real evolutionary networks. For each type of network, we show the complementary cumulative distribution function (CCDF) P_c of node rescaled degrees $k_{res} = k/\langle k \rangle$. Topological characteristics of this series of evolutionary networks are given in Table I.

different system sizes at five time points (see Table I), and these five networks all belong to phase III. Figure 6 shows the complementary cumulative degree distribution function of 10 types of real evolutionary networks; examining this characteristic, they are self-similar. The FFS analysis is performed along the RGN flow, and the results suggest that there is a phenomenon similar to that of synthetic networks, that is, the curves of each observable almost overlap under the scaling function with $n_l N_0^{1/\delta}$ as the variable, and the exponent $\delta \approx 2$ (see Figs. 7 and 8). The other nine types of evolutionary networks produced similar results (see Figs. S12– S29 in the Supplemental Material [45]).

IV. DISCUSSION

Based on the studies of Radicchi *et al.* [24] and García-Pérez *et al.* [27], this paper systematically studied the critical behavior of observables such as structure and dynamics of synthetic networks and real evolutionary networks from the perspective of RGN and FSS. Our results show that, influenced by the finite size of the network, excessive RGN iteration would lead to significant changes in the structure and dynamic characteristics of the network. However, this is not a disadvantage of RGN, because many networks have potential scale-invariant properties that are often masked by finite-size effects. For this purpose, this paper proves that the characteristic quantity of the network satisfies the scaling behavior in the process of RGN transformation with the help of FSS analysis and obtains the critical exponent that determines the universality class of the network.

In the process of RGN transformation, we do not pay attention to whether the network is self-similar or not, but project the network along the direction of RGN flow. The results show that the FSS can capture the universal scaling law that follows behind the projection, in which the critical exponent provides information that divides the small-world phase and non-small-world phase of the network from another perspective. According to our conclusion, RGN projection is suitable for both real evolutionary networks and static networks, especially for scale-free networks. Moreover, we can

learn many potential analysis methods from the RGN. For example, in large-scale simulations, the downscaled replica of the network can be used as an alternative or guidance to sampling methods or to quickly explore the critical behavior of a large-scale network. In addition, finite-size scaling can also be performed on the downscaled version of the real network, which would allow us to determine critical exponents from a single snapshot of the topology [27].

It should be noted that, similar to traditional FSS, the FSS analysis employed in this paper can also be used to estimate the scaling exponent of the diverging correlation length. Considering the differences between the $\mathbb{S}^1$ geometric model and the classical WS small-world model, we did not continue the relevant studies of Newman and Watts on diverging correlation length in small-world networks, a critical point at $p = 0$, and an associate finite-size scaling form [14]. Instead, FSS is used to reveal the scaling properties of network observables under the RGN flow. However, the relevant work is also very meaningful and deserves further research.

Finally, the RGN framework is developed on the basis of the hidden metric space model $\mathbb{S}^1/\mathbb{H}^2$ [27,28]. Like the box-covering method proposed by Song *et al.* [18], their core idea is coarse graining the network to reduce the size of the initial network. These methods have achieved good results for specific scenarios, but they all require special assumptions, such as embedding the network into space or based on the shortest path length [55]. Therefore, finding a robust way to rescale the network remains an open question. Another question is to what extent the conclusions of this paper depend on the specific assumptions of the $\mathbb{S}^1$ geometric model. To answer this question, a natural solution is to develop a renormalization group or sampling framework that does not require specific assumptions, and then explore whether there are similar laws behind it, which is very meaningful work. However, there are many challenges. For instance, although sampling schemes require no specific assumptions and are easy to operate, they tend to severely undermine the inherent structural characteristics of the initial network, such as scale-free, small-world, and modular properties. In contrast, the renormalization framework retains much of the basic properties of the original
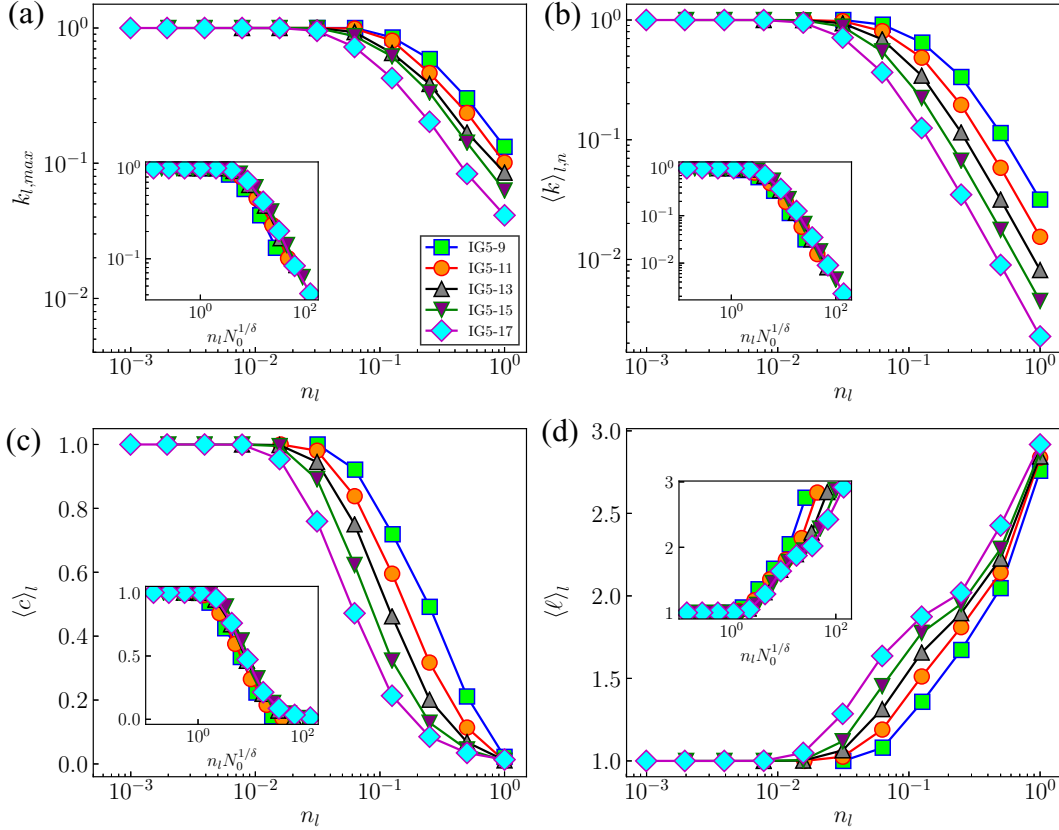
FIG. 7. FSS analysis of IG5 evolutionary networks' topological observables along the RGN flow. The main figures show each observable as a function of the variable n_l in the process of RGN transformation, and the inset shows their scaling functions related to the variable $n_l N_0^{1/\delta}$. These networks belong to phase III, and the scaling exponent corresponding to four observables is $\delta = 2.0(1)$.

network, but it requires specific assumptions. Therefore, we need to find a balanced solution to rescale the network and then explore the FSS properties, which is a direction that we need to pursue vigorously in the future.

V. CONCLUSION

In conclusion, the scaling behaviors of structural and dynamical observables of $\mathbb{S}^1$ synthetic and real evolutionary networks have been systematically investigated along the RGN flows. According to the structural properties of the $\mathbb{S}^1$ model, the network evolutionary phase can be divided into three regions. Some networks with different structural parameters are generated in each region, with finite-size scaling analysis on their structural and dynamical observables. The results show that these observables can be characterized by a certain scaling function with $n_l N_0^{1/\delta}$ as the variable. More importantly, the critical exponent δ is found to be independent of these observables but dependent only on the structural properties of the network.

Inspired by the findings on model $\mathbb{S}^1$, some real evolutionary network systems are considered, typically in the small-world phase, which also follows the finite-size scaling found in model $\mathbb{S}^1$. Specifically, for each system, there are different sizes at different time points. By embedding these networks of different sizes into the $\mathbb{S}^1$ network, it was found that they all approximate the same phase on the (ν, σ) plane, and these networks are self-similar. Thus, this investigation

continues to study the scaling laws of some real evolutionary systems in the same way as the synthetic networks. The findings further suggest that the $\mathbb{S}^1$ model can provide more evidence for predicting the structural and dynamical behavior of those real networks. On the other hand, the results of this paper can provide some guidance for studying the structural and functional characteristics of large-scale networks. For instance, an evolutionary network, often with a relatively small initial size, will eventually evolve to a large-scale system, so that it is difficult to obtain its structural and functional characteristics via computer simulation. While the scaling law found in this paper makes it possible to predict the characteristics of large-scale networks from small-size networks. Furthermore, the results also show that the RGN transformation may lead to significant changes of some properties of the network, which can be captured by the scaling function under the finite-size scaling analysis.
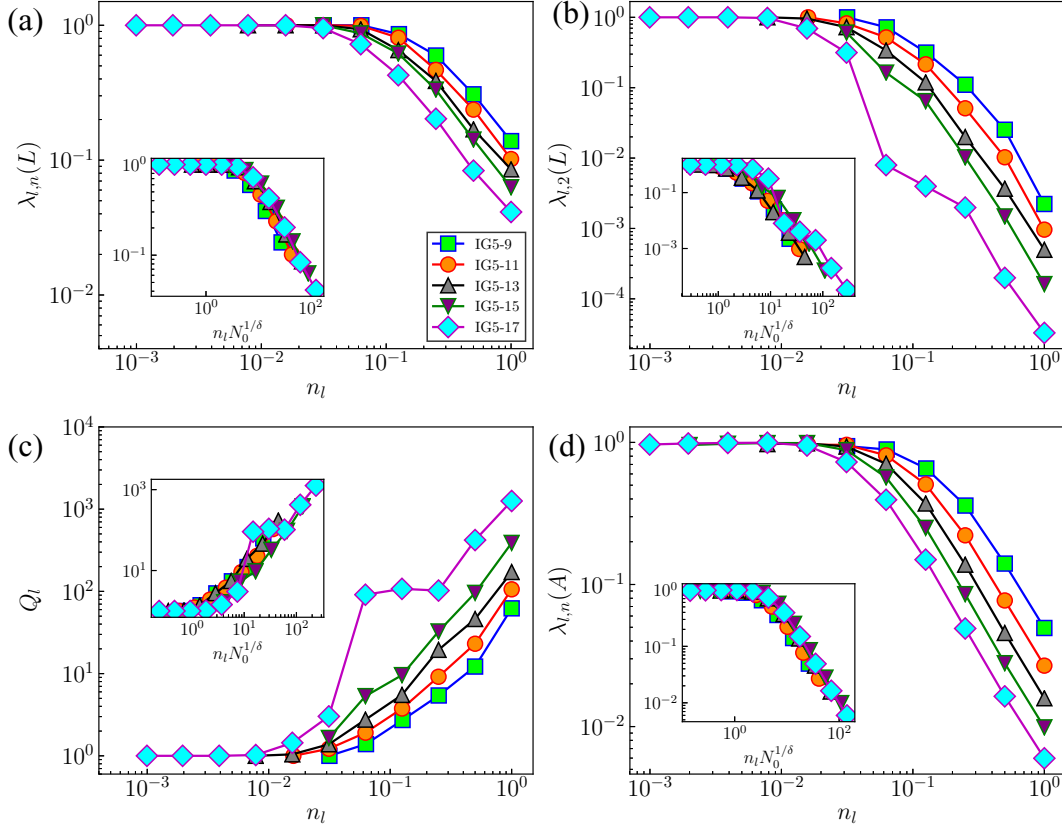
FIG. 8. FSS analysis of IG5 evolutionary networks' dynamic observables along the RGN flow. The main figures show each observable as a function of the variable n_l in the process of RGN transformation, and the inset shows their scaling functions related to the variable $n_l N_0^{1/\delta}$. The scaling exponent corresponding to four observables is $\delta = 2.0(1)$.

APPENDIX: NETWORK DATA SETS

We consider 10 types of evolutionary networks (including 39 networks): IG5, TF, Rajat, Gnutella peer-to-peer network [50,51,56], Cage, Maragal, Route Views AS graphs [52,57], CAIDA AS graphs (2004–2007) [52,58], and condensed mat-

ter collaborations [53,59], and Socfb-UC [49,60]. Among them, IG5, TF, Rajat, Cage, and Maragal [49] are collections of some miscellaneous networks; see [61]. The Socfb-UC network data set is in the category of Facebook networks. In this paper, we consider only the unweighted, undirected, and without self-loops versions of these networks. The basic topological characteristics of these networks are shown in Table I.

[1] S. Boccaletti, V. Latora, Y. Moreno, M. Chavez, and D.-U. Hwang, Complex networks: Structure and dynamics, Phys. Rep. **424**, 175 (2006).

[2] A.-L. Barabási, *Network Science* (Cambridge University Press, Cambridge, 2016).

[3] D. J. Watts and S. H. Strogatz, Collective dynamics of 'small-world' networks, Nature (London) **393**, 440 (1998).

[4] A.-L. Barabási and R. Albert, Emergence of scaling in random networks, Science **286**, 509 (1999).

[5] A. Arenas, A. Díaz-Guilera, J. Kurths, Y. Moreno, and C. Zhou, Synchronization in complex networks, Phys. Rep. **469**, 93 (2008).

[6] V. Nicosia, M. Valencia, M. Chavez, A. Díaz-Guilera, and V. Latora, Remote Synchronization Reveals Network Symmetries and Functional Modules, Phys. Rev. Lett. **110**, 174102 (2013).

[7] Y. Y. Liu, J. J. Slotine, and A.-L. Barabási, Controllability of complex networks, Nature (London) **473**, 167 (2011).

[8] Y. Y. Liu, J. J. Slotine, and A.-L. Barabási, Observability of complex systems, Proc. Natl. Acad. Sci. USA **110**, 2460 (2013).

[9] A. J. Whalen, S. N. Brennan, T. D. Sauer, and S. J. Schiff, Observability and Controllability of Nonlinear Networks: The Role of Symmetry, Phys. Rev. X **5**, 011005 (2015).

[10] V. Colizza, R. Pastor-Satorras, and A. Vespignani, Reaction-diffusion processes and metapopulation models in heterogeneous networks, Nat. Phys. **3**, 276 (2007).

[11] J. M. Kleinberg, Navigation in a small world, Nature (London) **406**, 845 (2000).

[12] E. López, S. V. Buldyrev, S. Havlin, and H. E. Stanley, Anomalous Transport in Scale-Free Networks, Phys. Rev. Lett. **94**, 248701 (2005).

[13] G. Li, S. D. S. Reis, A. A. Moreira, S. Havlin, H. E. Stanley, and J. S. Andrade, Towards Design Principles for Optimal Transport Networks, Phys. Rev. Lett. **104**, 018701 (2010).

[14] M. E. J. Newman and D. J. Watts, Renormalization group analysis of the small-world network model, Phys. Lett. A **263**, 341 (1999).

[15] L. P. Kadanoff, *Statistical Physics: Static, Dynamics and Renormalization* (World Scientific, Singapore, 2000).

[16] B. J. Kim, Geographical Coarse Graining of Complex Networks, Phys. Rev. Lett. **93**, 168701 (2004).

[17] D. Gfeller and P. De Los Rios, Spectral Coarse Graining of Complex Networks, Phys. Rev. Lett. **99**, 038701 (2007).

[18] C. Song, S. Havlin, and H. A. Makse, Self-similarity of complex networks, Nature (London) **433**, 392 (2005).

[19] C. Song, S. Havlin, and H. A. Makse, Origins of fractality in the growth of complex networks, Nat. Phys. **2**, 275 (2006).

[20] C. Song, L. K. Gallos, S. Havlin, and H. A. Makse, How to calculate the fractal dimension of a complex network: The box covering algorithm, J. Stat. Mech. (2007) P03006.

[21] K. I. Goh, G. Salvi, B. Kahng, and D. Kim, Skeleton and Fractal Scaling in Complex Networks, Phys. Rev. Lett. **96**, 018701 (2006).

[22] J. S. Kim, K. I. Goh, B. Hahng, and D. Kim, Fractality and self-similarity in scale-free networks, New. J. Phys. **9**, 177 (2007).

[23] J. S. Kim, K. I. Goh, G. Salvi, E. Oh, B. Kahng, and D. Kim, Fractality in complex networks: Critical and supercritical skeletons, Phys. Rev. E **75**, 016110 (2007).

[24] F. Radicchi, J. J. Ramasco, A. Barrat, and S. Fortunato, Complex Networks Renormalization: Flows and Fixed Points, Phys. Rev. Lett. **101**, 148701 (2008).

[25] F. Radicchi, A. Barrat, S. Fortunato, and J. J. Ramasco, Renormalization flows in complex networks, Phys. Rev. E **79**, 026104 (2009).

[26] H. D. Rozenfeld, C. Song, and H. A. Makse, Small-World to Fractal Transition in Complex Networks: A Renormalization Group Approach, Phys. Rev. Lett. **104**, 025701 (2010).

[27] G. García-Pérez, M. Boguñá, and M. Á. Serrano, Multiscale unfolding of real networks by geometric renormalization, Nat. Phys. **14**, 583 (2018).

[28] M. Á. Serrano, D. Krioukov, and M. Boguñá, Self-Similarity of Complex Networks and Hidden Metric Spaces, Phys. Rev. Lett. **100**, 078701 (2008).

[29] D. Krioukov, F. Papadopoulos, A. Vahdat, and M. Boguñá, Curvature and temperature of complex networks, Phys. Rev. E **80**, 035101(R) (2009).

[30] D. Krioukov, F. Papadopoulos, M. Kitsak, A. Vahdat, and M. Boguñá, Hyperbolic geometry of complex networks, Phys. Rev. E **82**, 036106 (2010).

[31] F. Papadopoulos, M. Kitsak, M. Á. Serrano, M. Boguñá, and D. Krioukov, Popularity versus similarity in growing networks, Nature (London) **489**, 537 (2012).

[32] M. Boguñá, F. Papadopoulos, and D. Krioukov, Sustaining the internet with hyperbolic mapping, Nat. Commun. **1**, 1 (2010).

[33] A. Allard, M. Á. Serrano, G. García-Pérez, and M. Boguñá, The geometric nature of weights in real complex networks, Nat. Commun. **8**, 14103 (2017).

[34] A. Brouwer, *Spectra of Graphs* (Springer, New York, 2012).

[35] T. Nishikawa, J. Sun, and A. E. Motter, Sensitive Dependence of Optimal Network Dynamics on Network Structure, Phys. Rev. X **7**, 041044 (2017).

[36] T. Nishikawa, A. E. Motter, Y.-C. Lai, and F. C. Hoppensteadt, Heterogeneity in Oscillator Networks: Are Smaller Worlds Easier to Synchronize, Phys. Rev. Lett. **91**, 014101 (2003).

[37] L. Donetti, P. I. Hurtado, and M. A. Muñoz, Entangled Networks, Synchronization, and Optimal Network Topology, Phys. Rev. Lett. **95**, 188701 (2005).

[38] T. Nishikawa and A. E. Motter, Synchronization is optimal in nondiagonalizable networks, Phys. Rev. E **73**, 065106(R) (2006).

[39] T. Nishikawa and A. E. Motter, Maximum performance at minimum cost in network synchronization, Physica (Amsterdam) D **224**, 77 (2006).

[40] M. Brede, Optimal synchronization in space, Phys. Rev. E **81**, 025202(R) (2010).

[41] M. Barahona and L. M. Pecora, Synchronization in Small-World Systems, Phys. Rev. Lett. **89**, 054101 (2002).

[42] D. H. Shi, G. Chen, W. W. K. Thong, and X. Yan, Searching for optimal network topology with best possible synchronizability, IEEE Circ. Sys. Mag. **13**, 66 (2013).

[43] C. Castellano and R. Pastor-Satorras, Relating Topological Determinants of Complex Networks to Their Spectral Properties: Structural and Dynamical Effects, Phys. Rev. X **7**, 041024 (2017).

[44] J. G. Restrepo, E. Ott, and B. R. Hunt, Onset of synchronization in large networks of coupled oscillators, Phys. Rev. E **71**, 036151 (2005).

[45] See Supplemental Material at http://link.aps.org/supplemental/10.1103/PhysRevE.104.034304 for additional FFS analysis results include synthetic networks in other regions, high-dimensional embedded networks, and other nine types of real evolutionary networks.

[46] Here we need to measure the quality S of the collapse plot, which is defined as the mean square distance between the data and the master curve [47,48]. When S gets the minimum value, the collapse quality of different curves is the best and corresponds to an optimal δ. It should be noted that considering external factors such as statistical errors, the optimal critical exponent δ corresponding to each observable is not strictly equal.

[47] J. Houdayer and A. K. Hartmann, Low-temperature behavior of two-dimensional Gaussian Ising spin glasses, Phys. Rev. B **70**, 014418 (2004).

[48] O. Melchert, autoScale.py—A program for automatic finite-size scaling analyses: A user's guide, arXiv:0910.5403 (2009).

[49] R. A. Rossi and N. K. Ahmed, The network data repository with interactive graph analytics and visualization, in *Proceedings of the 29th AAAI Conference on Artificial Intelligence* (AIAA, Reston, VA, 2015).

[50] J. Leskovec, J. Kleinberg, and C. Faloutsos, Graph evolution: Densification and shrinking diameters, in *ACM Transactions on Knowledge Discovery from Data (TKDD)* (ACM, New York, 2007).

[51] M. Ripeanu, I. Foster, and A. Iamnitchi, Mapping the gnutella network: Properties of large-scale peer-to-peer systems and implications for system design, *IEEE Internet Comput.* (IEEE, Piscataway, NJ, 2002), Vol. 6.

[52] J. Leskovec, J. Kleinberg, and C. Faloutsos, Graphs over time: Densification laws, shrinking diameters and possible

explanations, in *Proceedings of the Eleventh ACM SIGKDD International Conference on Knowledge Discovery in Data Mining* (ACM, New York, 2005), pp. 177–187.

[53] M. E. Newman, The structure of scientific collaboration networks, Proc. Natl. Acad. Sci. USA **98**, 404 (2001).

[54] G. García-Pérez, A. Allard, M. Á. Serrano, and M. Boguñá, Mercator: Uncovering faithful hyperbolic embeddings of complex networks, New J. Phys. **21**, 123033 (2019).

[55] M. Serafino, G. Cimini, A. Maritan, A. Rinaldo, S. Suweis, J. R. Banavar, and G. Caldarelli, True scale-free networks hidden by finite size effects, Proc. Natl. Acad. Sci. USA **118**, e2013825118 (2021).

[56] http://snap.stanford.edu/data/.

[57] http://snap.stanford.edu/data/as.html.

[58] http://snap.stanford.edu/data/as-caida.html.

[59] http://www-personal.umich.edu/~mejn/netdata/.

[60] http://networkrepository.com/socfb.

[61] http://networkrepository.com/misc.php.